

Preparation of AlN film grown on sputter-deposited and annealed AlN buffer layer via HVPE

Di-Di Li(李迪迪), Jing-Jing Chen(陈晶晶), Xu-Jun Su(苏旭军), Jun Huang(黄俊), Mu-Tong Niu(牛牧童), Jin-Tong Xu(许金通), and Ke Xu(徐科)

Citation: Chin. Phys. B, 2021, 30 (**3**): 036801. DOI: 10.1088/1674-1056/abd392
Journal homepage: http://cpb.iphy.ac.cn; http://iopscience.iop.org/cpb

What follows is a list of articles you may be interested in

Influence comparison of N_2 and NH_3 nitrogen sources on AlN films grown by halide vapor phase epitaxy

Jing-Jing Chen(陈晶晶), Jun Huang(黄俊), Xu-Jun Su(苏旭军), Mu-Tong Niu(牛牧童), Ke Xu(徐科)
Chin. Phys. B, 2020, 29 (**7**): 076802. DOI: 10.1088/1674-1056/ab90ed

PEALD-deposited crystalline GaN films on Si (100) substrates with sharp interfaces

San-Jie Liu(刘三姐), Ying-Feng He(何荧峰), Hui-Yun Wei(卫会云), Peng Qiu(仇鹏), Yi-Meng Song(宋祎萌), Yun-Lai An(安运来), Abdul Rehman(阿布度-拉赫曼), Ming-Zeng Peng(彭铭曾), Xin-He Zheng(郑新和)
Chin. Phys. B, 2019, 28 (**2**): 026801. DOI: 10.1088/1674-1056/28/2/026801

Growth condition optimization and mobility enhancement throughprolonging the GaN nuclei coalescence process of AlGaN/AlN/GaN structure

He Xiao-Guang, Zhao De-Gang, Jiang De-Sheng, Zhu Jian-Jun, Chen Ping, Liu Zong-Shun, Le Ling-Cong, Yang Jing, Li Xiao-Jing, Zhang Shu-Ming, Yang Hui
Chin. Phys. B, 2015, 24 (**9**): 096802. DOI: 10.1088/1674-1056/24/9/096802

Characterization of tetragonal distortion in a thick $Al_{0.2}Ga_{0.8}N$ epilayer with an AlN interlayer by Rutherford backscattering/channeling

Wang Huan, Yao Shu-De
Chin. Phys. B, 2014, 23 (**9**): 096801. DOI: 10.1088/1674-1056/23/9/096801

First-principles calculations of 5d atoms doped hexagonal-AlN sheets：Geometry, magnetic property and the influence of symmetry and symmetry-breaking on the electronic structure

Zhang Zhao-Fu, Zhou Tie-Ge, Zhao Hai-Yang, Wei Xiang-Lei
Chin. Phys. B, 2014, 23 (**1**): 016801. DOI: 10.1088/1674-1056/23/1/016801

Preparation of AlN film grown on sputter-deposited and annealed AlN buffer layer via HVPE*

Di-Di Li(李迪迪)[1,3], Jing-Jing Chen(陈晶晶)[1,3], Xu-Jun Su(苏旭军)[1], Jun Huang(黄俊)[1], Mu-Tong Niu(牛牧童)[1], Jin-Tong Xu(许金通)[4], and Ke Xu(徐科)[1,2,3,†]

[1] *Suzhou Institute of Nano-tech and Nano-bionics, Chinese Academy of Sciences, Suzhou* 215123, *China*
[2] *Suzhou Nanowin Science and Technology Co., Ltd., Suzhou* 215123, *China*
[3] *School of Physical Science and Technology, ShanghaiTech University, Shanghai* 201210, *China*
[4] *Key Laboratory of Infrared Imaging Materials and Detectors, Shanghai Institute of Technical Physics, Chinese Academy of Sciences, Shanghai* 200083, *China*

(Received 13 September 2020; revised manuscript received 13 November 2020; accepted manuscript online 15 December 2020)

AlN films grown on sputter-deposited and annealed AlN buffer layer by high temperature hydride vapor phase epitaxy (HVPE) have been fabricated and structurally characterized. The crystalline quality and surface morphology of as-grown AlN films with various V/III ratios were studied and compared. The XRD results showed that the crystalline quality of the AlN film could be optimized when the growth V/III ratio was 150. At the same time, the full width at half-maximum (FWHM) values of (0002)- and (10$\bar{1}$2)-plane were 64 arcsec and 648 arcsec, respectively. As revealed by AFM, the AlN films grown with higher V/III ratios of 150 and 300 exhibited apparent hillock-like surface structure due to the low density of screw threading dislocation (TD). The defects microstructure and strain field around the HVPE-AlN/sputtered-AlN/sapphire interfaces have been investigated by transmission electron microscopy (TEM) technique combined with geometric phase analysis (GPA). It was found that the screw TDs within AlN films intend to turn into loops or half-loops after originating from the AlN/sapphire interface, while the edge ones would bend first and then reacted with others within a region of 400 nm above the interface. Consequently, part of the edge TDs propagated to the surface vertically. The GPA analysis indicated that the voids extending from sapphire to HVPE-AlN layer were beneficial to relax the interfacial strain of the best quality AlN film grown with a V/III ratio of 150.

Keywords: hydride vapor phase epitaxy (HVPE), AlN, threading dislocation (TD), sputter-deposition

PACS: 68.55.−a, 81.15.−z, 61.72.−y **DOI:** 10.1088/1674-1056/abd392

1. Introduction

Recently, high quality AlN film has attracted a lot of interest due to its outstanding characteristics, like wide bandgap (6.2 eV), high surface acoustic wave velocity (5760 m/s in the *c*-plane), good thermal and chemical stability.[1,2] Especially, high quality AlN is crucial in fabricating deep-ultraviolet light-emitting diodes (DUV-LED) and laser diodes (LD), which play an important role in the field of water purification, medical treatment, and communication.[3] However, high threading dislocation density (TDD) of AlN would reduce the internal quantum efficiency (IQE) of DUV-LED.[4] In addition, pure screw threading dislocations would act as the leakage path in p–n diodes.[5] Therefore, it is significant to fabricate high quality AlN with low TDD for the application.

Homoepitaxy is considered as an ideal method to grow high quality AlN films with low TDD due to the same lattice constant and thermal expansion coefficient between the substrate and epilayer.[6,7] Nevertheless, the heteroepitaxy strategy is more widely used, ascribing to the lack of natural intrinsic substrates. As is well-known, the sapphire is the most commonly used substrates for fabricating AlN template due to its high UV-transparency and low cost. Many researchers have devoted tremendous effort to improve the quality of AlN film on sapphire substrates, such as the multi-step growth[8–10] and epitaxial lateral overgrowth on patterned sapphire substrates.[11,12] However, TDDs of the AlN films are still among the order of 10^9–10^{10} cm^{-2}, due to the poor Al adatom mobility.[13] Miyake *et al.* proposed that overlapped "face-to-face" high-temperature (HT) annealing could suppress the thermal decomposition of the AlN films, which is effective in reducing the TDD.[14] They have succeeded in fabricating high quality AlN by combing MOVPE with a sputter-deposited annealed AlN buffer layer. However, there are few reports about growing AlN films on sputter-deposited and annealed AlN layer by hydride vapor phase epitaxy (HVPE). A detailed investigation of it is important for the stable growth of high-quality AlN films.

In this report, the AlN films were prepared on a sputter-deposited AlN buffer layer, which was annealed at a high temperature of 1500 °C, with a home-built horizontal HVPE system. The dependence of the surface morphology, crystallinity, and microstructure of the HVPE-AlN layer on various growth V/III ratios was investigated, which would be beneficial for the

*Project supported by the National Key Technologies R&D Program of China (Grant No. 2017YFB0404100) and Key Laboratory of Infrared Imaging Materials and Detectors, Shanghai Institute of Technical Physics, Chinese Academy of Sciences.

†Corresponding author. E-mail: kxu2006@sinano.ac.cn

© 2021 Chinese Physical Society and IOP Publishing Ltd

growth of high-quality AlN films.

2. Experiments

25 nm-thick AlN layers were sputtered on 2-inch c-plane sapphire substrates by sputtering technology. The radio frequency power and growth temperature were 750 W and 650 °C, respectively. The AlN thick films with average thicknesses of about 5.5 μm were then grown on sputtered AlN buffer layers in a home-built HVPE system by the following procedures: initially, the 25 nm-thick sputtered AlN/sapphire was heated to 1500 °C in flowing NH_3, and then annealed in an H_2 and N_2 mixture atmosphere with a total chamber pressure of 20 hPa for 30 min. After that, a 5.5 μm-thick AlN film was grown on sputter-deposited annealed AlN/sapphire by HVPE. In the experiments, the reactor chamber was maintained at 10 hPa, the $AlCl_3$ and N_2 flow rates were 50 and 200 sccm, respectively, and the carrier H_2 flow rates were 2000 sccm. $AlCl_3$ was generated in the reactor (source zone) by the reaction between Al metal and HCl gas at 500 °C. In this work, three samples grown with different V/III ratios were compared, and their growth conditions were shown in Table 1. The V/III ratio, namely, the $N_2/AlCl_3$ratio, was calculated by the input flux ratio of N_2 and HCl gas, assuming that HCl fully reacted with metal Al to form $AlCl_3$.

High-resolution x-ray diffraction (Bruker D8 Discover, EUR) was used to characterize the crystal quality of the AlN films. Atomic force microscopy (Veeco Dimension ICON, USA) was applied to measure the surface morphology of the AlN films in tapping mode. The microstructure observations were performed on a transmission electron microscope (TALOS F200X, USA) with an accelerating voltage of 200 kV. The cross-sectional specimens for TEM measurements were prepared by mechanical polishing and followed by the Ar^+ ion milling process.

Table 1. Growth conditions of as-grown AlN samples, as well as the full width at half-maximum (FWHM) value of (0002) and ($10\bar{1}2$) plane x-ray rocking curves (XRCs) for HVPE-AlN films.

Sample	Annealing temperature (°C)	HCl flux (sccm)	N_2 flux (sccm)	V/III ratio	$FWHM_{0002}$ (arcsec)	$FWHM_{10\bar{1}2}$ (arcsec)
A	1500	0.03	0.5	100	294	652
B	1500	0.02	0.5	150	64	648
C	1500	0.01	0.5	300	165	682

3. Results and discussion

To evaluate the crystalline quality of as-fabricated AlN samples with different V/III ratios, the x-ray rocking curves (XRCs) of the symmetric (0002) and asymmetric ($10\bar{1}2$) diffractions for three AlN samples from A to C were conducted, respectively, with the corresponding full width at half-maximum (FWHM) values derived, as shown in Fig. 1. The following equations can be used to further estimate the density of screw and edge dislocations for AlN samples:[15,16]

$$\rho_{\text{screw}} = \beta_{\text{tilt}}^2/4.35b_{\text{c}}^2, \quad \rho_{\text{edge}} = \beta_{\text{twist}}^2/4.35b_{\text{a}}^2, \tag{1}$$

$$\beta_{\omega}^2 = (\beta_{0002}\cos\chi)^2 + (\beta_{10\bar{1}0}\cos\chi)^2, \tag{2}$$

where β_{tilt} and β_{twist} are the tilt and twist angle of (0002) and ($10\bar{1}0$) planes and are expressed in radian; b_{c} and b_{a} are the burgers vectors of c-type and a-type threading dislocations, respectively; $\beta_{10\bar{1}0}$ can be calculated by Eq. (2) and χ is the angle between ($10\bar{1}2$) plane and the normal line of (0001) basal plane.

As shown in Fig. 1(c), the FWHM values of (0002) plane for samples A–C are 294, 64, and 165 arcsec, corresponding to the density of screw TD of about 1.9×10^8, 8.9×10^6, and 5.9×10^7 cm^{-2}, respectively. Meanwhile, the FWHM values of ($10\bar{1}2$) plane for samples A-C are 652, 648, and 682 arcsec, corresponding to a density of edge TD of about 4.6×10^9, 5.1×10^9, and 5.5×10^9 cm^{-2}, respectively. It suggests that sample B, with the growth V/III ratio of 150, has the narrowest FWHMs, namely the best crystalline quality. Figure 1(d) shows the orientation of the sputtered AlN buffer layer before high-temperature annealing. It can be found that the (0002) and (0004) peaks of AlN and (0006) peaks of Al_2O_3 are obvious, indicating the high *c*-axis orientation of the sputtered-AlN buffer layer.

Figure 2 presents the AFM images of AlN samples from A to C, respectively, to reveal the morphology evolution of samples with V/III ratios increasing. The insets are the magnified AFM images. As shown by Fig. 2(a), sample A grown at a V/III ratio of 100 shows uncoalesced hexagonal islands on the surface. When the V/III ratio is higher than 150, AlN films show hillock-like surface structure, as seen in Figs. 2(b) and 2(c). This can be attributed to the low density of screw TD and mixed TD with screw-component, since the high density screw and mixed TD would impede the lateral enlargement of spiral growth, and thus the hillocks form on the AlN surface.[17,18] According to the previous XRD results, sample B has the narrowest FWHM of (0002) plane, which means the smallest density of screw TD. Namely, sample B has the smallest spiral growth resistance, which would facilitate the formation of the hillock structure, while the opposite case is true in sample A. In addition, the root mean square (RMS) values of surface roughness for samples (see the insets) are 4.69, 0.75, and 0.20 nm, respectively. Obviously, the surface roughness of the HVPE-AlN decreases when the V/III ratio of the regrowth increases.

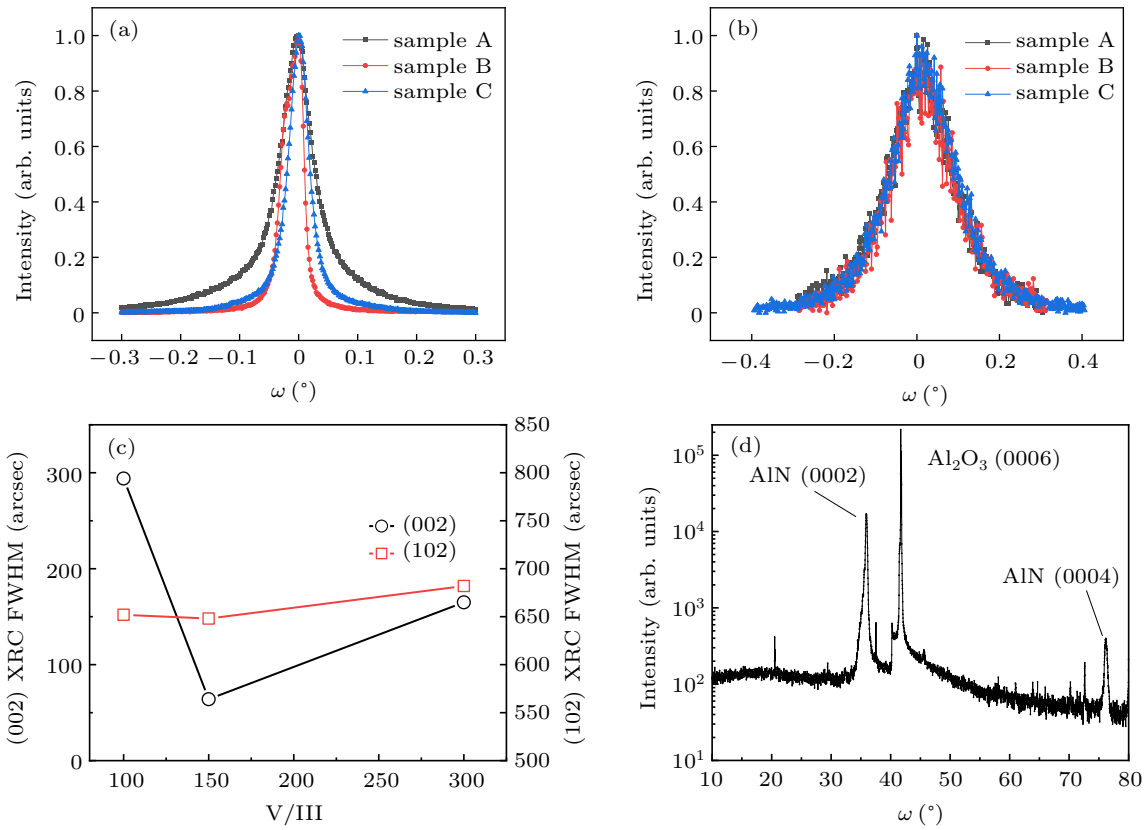


Fig. 1. XRD rocking curves of (a) AlN (0002) plane and (b) $(10\bar{1}2)$ plane for AlN samples with different V/III ratios, (c) FWHMs of (0002) plane and $(10\bar{1}2)$ plane for AlN samples based on (a) and (b), respectively. (d) The full XRD pattern of the 25 nm thick sputtered-AlN buffer layer before high-temperature annealing.

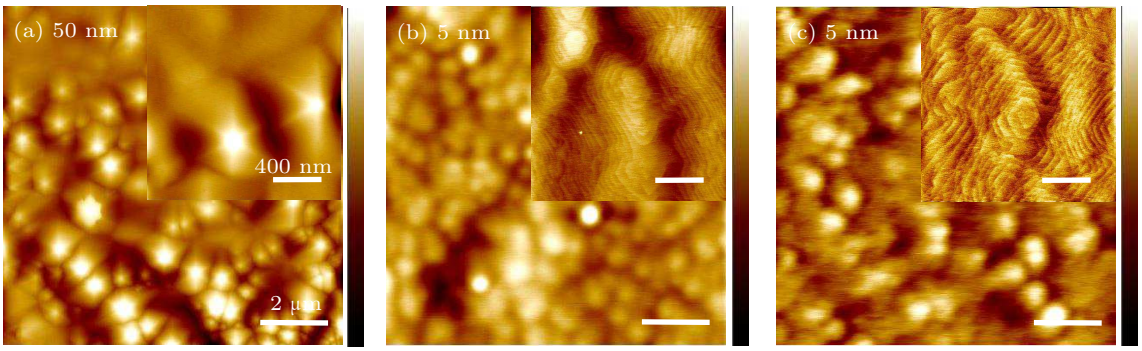


Fig. 2. AFM images of the HVPE-AlN films grown on sputter-deposited and annealed AlN buffer layer: (a) sample A, (b) sample B, and (c) sample C. The insets present the magnified AFM images of the samples, correspondingly. The scale bars are 2 μm, while 400 nm in the inset. The height of morphology is indicated by color scales at the right side of each image, where 50, 5, and 5 nm are the maximum value of the color scales.

In order to elucidate the evolution of TDs within AlN films grown with varied V/III ratios, the as-grown AlN samples are prepared into cross-sectional specimens for TEM observation. Figure 3 presents the weak beam dark field (WBDF) images of cross-section samples A–C, with different imaging diffraction vectors of $\boldsymbol{g} = 0002$ and $\boldsymbol{g} = 11\bar{2}0$, respectively. Figure 3 also indicates that the average thickness of the as-grown AlN films is about 5.5 μm. According to the visible-invisible criterion,[19] the vector of $\boldsymbol{g} = 0002$ is commonly used to observe screw-component TDs, and $\boldsymbol{g} = 11\bar{2}0$ to identify the edge-component TDs. Figures 3(a)–3(c), taken at $\boldsymbol{g} = 0002$, show that there are few screw TDs in the AlN samples, and most of those screw TDs are loops or half-loops. Those half-loops are obviously originated from the AlN/sapphire interface and expand in $\{1\bar{1}00\}$ planes. Figures 3(d)–3(f), taken at $\boldsymbol{g} = 11\bar{2}0$, suggest that the TDs are dominantly edge-component in the AlN samples, which is consistent with the result of XRD. Those edge TDs originate from the AlN/sapphire interface and propagate to the surface. Edge TDs near the AlN/sapphire interface are too many to be distinguished from each other. However, near the surface, they are obviously perpendicular to the (0001) plane.

To improve the TDs imaging quality, the typical high magnification WBDF images of the AlN/sapphire interface are

presented in Fig. 4. As illustrated by Fig. 4, the edge TDs near the AlN/sapphire interface in the AlN samples have different propagation behavior. Specifically, edge TDs in samples A and B bend slightly in the first 400 nm region above AlN/sapphire interface (see Figs. 4(a) and 4(b)). However, the TDs in sample C are mostly vertical to the (0001) basal plane (see Fig. 4(c)). Compared with sample C, TDs stand a better chance to interact with each other in samples A and B before propagating to the surface. This may explain the fact that the sample C with the highest V/III ratio has the highest TDD among the three samples, and the lower V/III ratio would improve the crystal quality.[20]

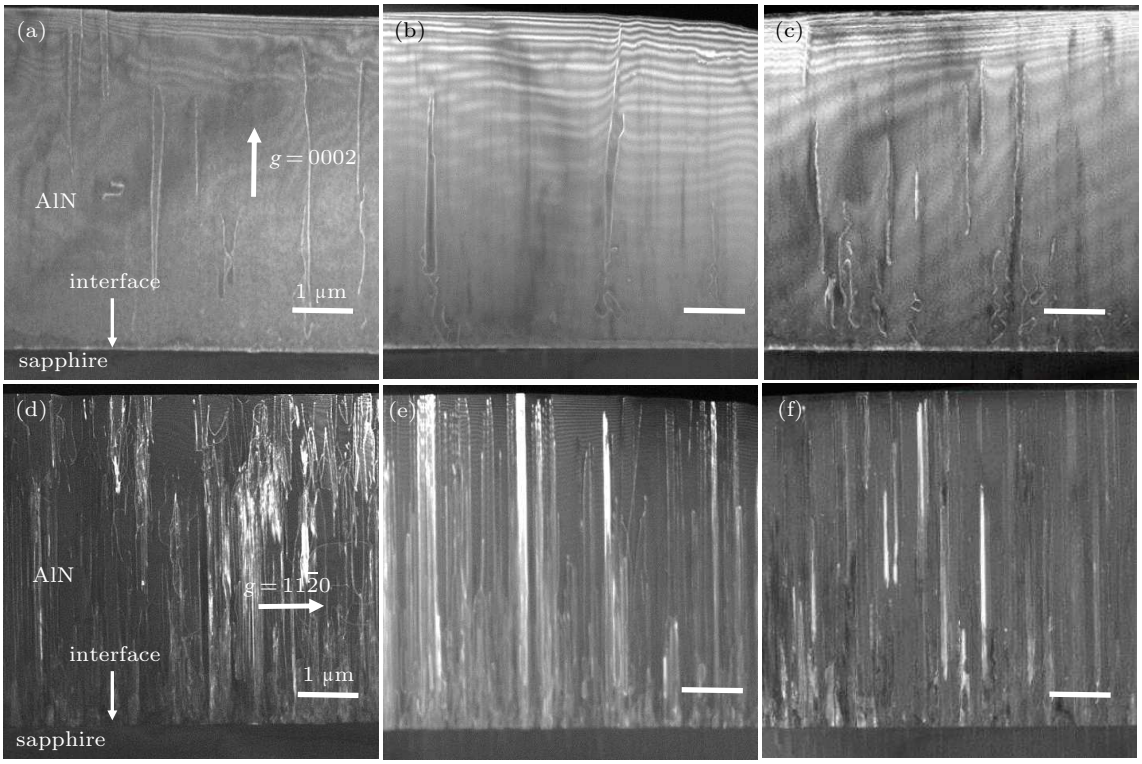


Fig. 3. Cross-sectional weak beam dark field (WBDF) images under the two-beam condition: (a) and (d) for sample A, (b) and (e) for sample B, (c) and (f) for sample C. The upper row images are recorded with g vector of $\boldsymbol{g} = 0002$, and the lower row images are recorded with $\boldsymbol{g} = 11\bar{2}0$. The scale bars are 1 μm.

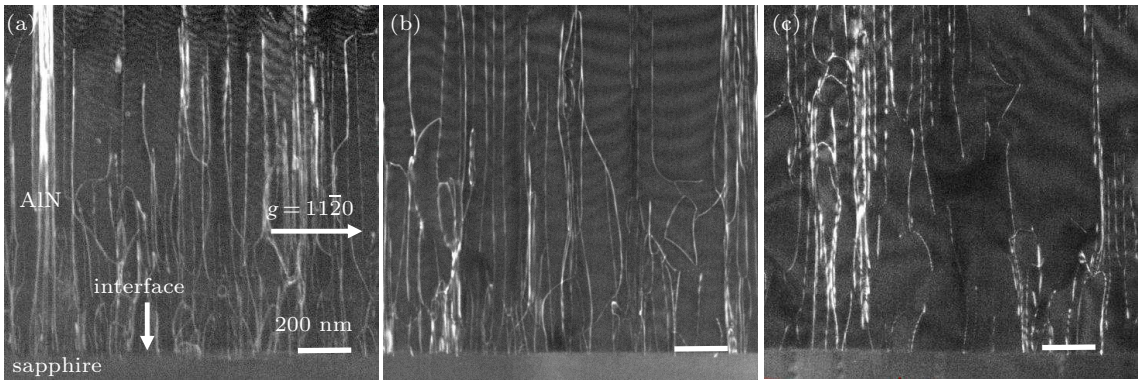


Fig. 4. Weak beam dark field images (WBDF) of the AlN/sapphire interface: (a) for sample A, (b) for sample B, and (c) for sample C. The images are recorded with g vector of $\boldsymbol{g} = 11\bar{2}0$, and the scale bars are 200 nm.

The strain distribution near the HVPE-AlN/sputtered-AlN/sapphire interfaces for AlN samples has been analyzed by high resolution transmission electron microscopy (HRTEM) combined with geometric phase analysis (GPA),[21] based on the slight distortion of lattice fringes in HRTEM, as shown in Fig. 5. Figures 5(a), 5(c) and 5(e) are the HRTEM images of HVPE-AlN/sputtered-AlN/sapphire interfaces for sample A–C, respectively. In addition, the selected area electron diffraction (SAED) shows the orientation of the sputtered-AlN after high-temperature annealing (shown insets). The sputter-deposited and annealed AlN buffer layers are indicated by two black lines.

The thickness of the sputter-deposited annealed AlN buffer layer in Fig. 5 is less than 25 nm, attributed to the decomposition of the AlN sputter layer during the high temperature annealing and growth. Simultaneously, the HVPE-

AlN/sputtered-AlN/sapphire interfaces become rough with voids of different sizes generating around them in samples. The nano-voids are speculated to be caused by the decomposition of sputtered-AlN[22] or sapphire (Al_2O_3)[23] during the high temperature annealing process. The decomposition of sapphire (Al_2O_3) at high temperature (above 1300 °C) is a common phenomenon, and the decomposition is governed by the following chemical reaction:[24,25] Al_2O_3 (s) + $3H_2$(g) = 2Al (g) + $3H_2O$ (g).

The GPA images of samples, corresponding to Figs. 5(a), 5(c) and 5(e), are shown in Figs. 5(b), 5(d) and 5(f), respectively, with extracted strain data from white dot lines in them on their right side. From the extracted strain data, it can be found that the sputtered-AlN/sapphire interfaces and HVPE-AlN/sputtered-AlN interface in sample A and sample C are the strain concentration area. However, there is no large strain at the sputtered-AlN/HVPE-AlN interface of sample B. It is probably caused by the unique shape of voids in sample B, which extend from sapphire to HVPE-AlN and provide more space for the strain relaxation, leading to less TDs generation at interfaces. The SAED reveals that the sputtered-AlN grown on sapphire after high-temperature annealing takes the epitaxial relationship of AlN(11$\bar{2}$0)//Al_2O_3(01$\bar{1}$0) and AlN(0002)//Al_2O_3(0006). As mentioned previously, the sample A–C are only different in growth V/III ratio, and it is still unclear whether it would result in the different voids generating at interfaces of samples. The related study is still ongoing.

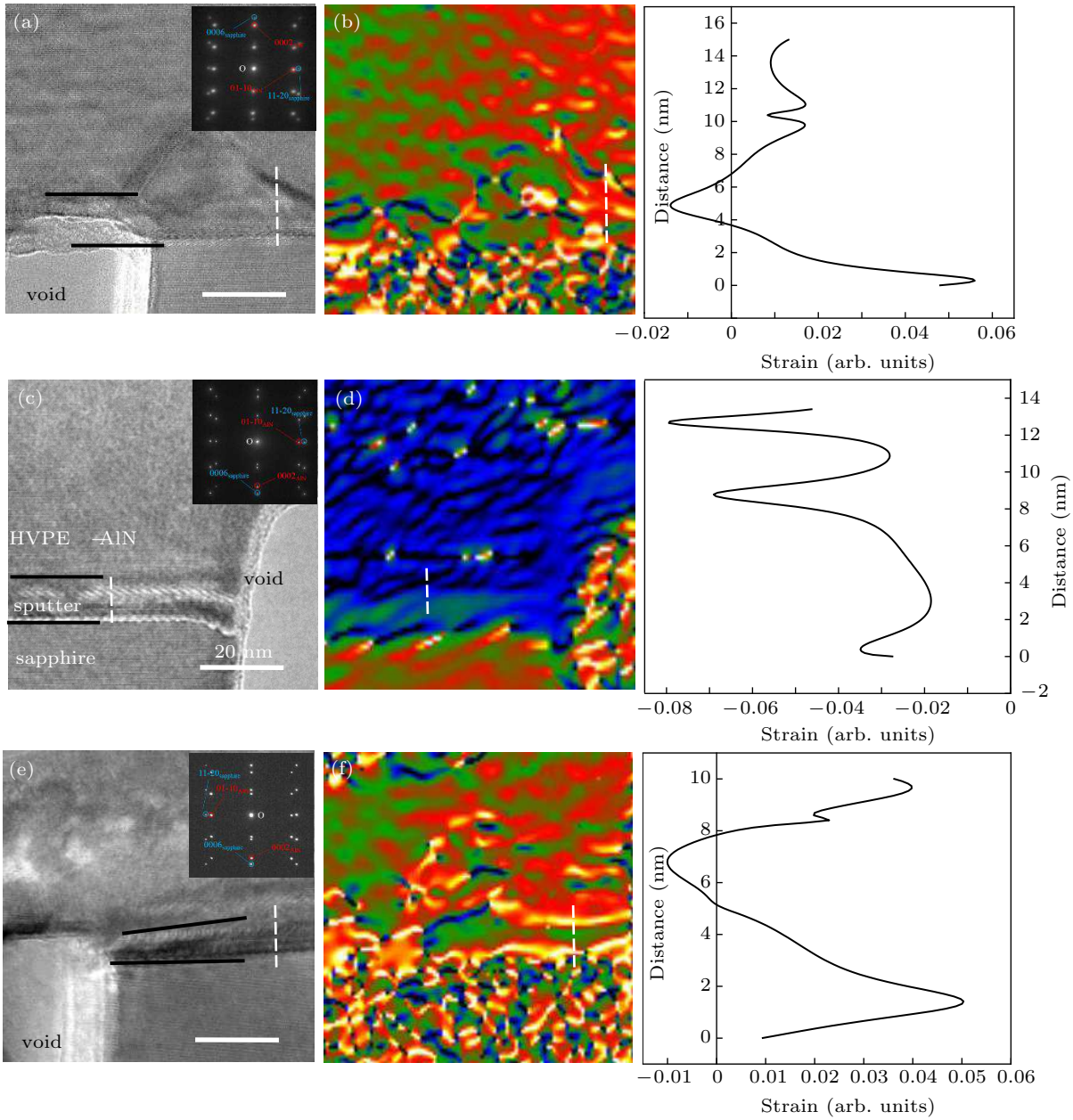


Fig. 5. Cross-sectional high resolution transmission electron microscopy (HRTEM) images of HVPE-AlN/sputtered-AlN/sapphire interfaces (a) for sample A, (c) for sample B, and (e) for sample C; (b), (d) and (f) are the GPA images corresponding to the (a), (c) and (e), respectively, with the extracted strain data along the white dot lines in them on their right sides. The insets are the selected area electron diffraction patterns near the interface. The incident beam is along the [11$\bar{2}$0] zone axis and the scale bars are 20 nm.

4. Conclusion

In summary, AlN films grown on the sputter-deposited and annealed AlN buffer layer, by high-temperature (HVPE), have been fabricated at different V/III ratios. When the growth V/III ratio is 150, the crystalline quality of AlN films can be optimized in our experiments, and the XRC FWHM values of (0002)- and $(10\bar{1}2)$-planes are 64 and 648 arcsec, respectively. According to AFM observations, the higher growth V/III ratio would be beneficial to the hillock structure formation of AlN films, probably due to the low density of screw and mixed TDs. Otherwise, the uncoalesced islands structure would appear. The screw TDs in the as-grown AlN films obliquely form loops or half-loops after generation. Therefore, the TDs reaching to the surface of AlN films are mainly the edge TDs. Finally, after the high-temperature annealing, the HVPE-AlN/sputtered-AlN/sapphire interfaces get rougher and voids of different sizes generate around them. For the best crystalline quality sample, the voids are big enough to extend from sapphire to HVPE-AlN, which would be beneficial to relax the interface strain, and thus improving the crystalline quality of samples.

References

[1] Wang M X, Xu F J, Xie N, Sun Y H, Liu B Y, Qin Z X, Wang X Q and Shen B 2018 *Cryst Eng. Comm.* **20** 6613

[2] Deger C, Born E, Angerer H, Ambacher O, Stutzmann M, Hornsteiner J, Riha E and Fischerauer G 1998 *Appl. Phys. Lett.* **72** 2400

[3] Huang C Y, Wu P Y, Chang K S, Lin Y H, Peng W C, Chang Y Y, Li J P, Yen H W, Wu Y S, Miyake H and Kuo H C 2017 *AIP Adv.* **7** 055110

[4] Kinoshita T, Hironaka K, Obata T, Nagashima T, Dalmau R, Schlesser R, Moody B, Xie J, Inoue S i, Kumagai Y, Koukitu A and Sitar Z 2012 *Appl. Phys. Express* **5** 122101

[5] Usami S, Ando Y, Tanaka A, Nagamatsu K, Deki M, Kushimoto M, Nitta S, Honda Y, Amano H, Sugawara Y, Yao Y Z and Ishikawa Y 2018 *Appl. Phys. Lett.* **112** 182106

[6] Yan J, Wang J, Zhang Y, Cong P, Sun L, Tian Y, Zhao C and Li J 2015 *J. Cryst. Growth* **414** 254

[7] Dong P, Yan J, Wang J, Zhang Y, Geng C, Wei T, Cong P, Zhang Y, Zeng J, Tian Y, Sun L, Yan Q, Li J, Fan S and Qin Z 2013 *Appl. Phys. Lett.* **102** 241113

[8] Bai J, Dudley M, Sun W H, Wang H M and Khan M A 2006 *Appl. Phys. Lett.* **88** 051903

[9] He C, Zhao W, Wu H, Zhang S, Zhang K, He L, Liu N, Chen Z and Shen B 2018 *Crystal Growth & Design* **18** 6816

[10] Imura M, Fujimoto N, Okada N, Balakrishnan K, Iwaya M, Kamiyama S, Amano H, Akasaki I, Noro T, Takagi T and Bandoh A 2007 *J. Cryst. Growth* **300** 136

[11] Zhang L, Xu F, Wang J, He C, Guo W, Wang M, Sheng B, Lu L, Qin Z, Wang X and Shen B 2016 *Sci. Rep.* **6** 35934

[12] Xiao S, Jiang N, Shojiki K, Uesugi K and Miyake H 2019 *Jpn. J. Appl. Phys.* **58** SC1003

[13] Huang J, Niu M T, Zhang J C, Wang W, Wang J F and Xu K 2017 *J. Cryst. Growth* **459** 159

[14] Miyake H, Lin C H, Tokoro K and Hiramatsu K 2016 *Journal of Crystal Growth* **456** 155

[15] Taniyasu Y, Kasu M and Makimoto T 2007 *J. Cryst. Growth* **298** 310

[16] Liu J Q, Wang J F, Liu Y F, Huang K, Hu X J, Zhang Y M, Xu Y, Xu K and Yang H 2009 *J. Cryst. Growth* **311** 3080

[17] Uesugi K, Shojiki K, Tezen Y, Hayashi Y and Miyake H 2020 *Appl. Phys. Lett.* **116** 062101

[18] Heying B, Tarsa E J, Elsass C R, Fini P, DenBaars S P and Speck J S 1999 *J. Appl. Phys.* **85** 6470

[19] Su X, Zhang J, Huang J, Zhang J, Wang J and Xu K 2017 *J. Cryst. Growth* **467** 82

[20] Severino A and Iucolano F 2016 *Physica Status Solidi (b)* **253** 801

[21] Ben J, Shi Z, Zang H, Sun X, Liu X, Lü W and Li D 2020 *Appl. Phys. Lett.* **116** 251601

[22] Huang J, Niu M, Sun M, Su X and Xu K 2019 *Cryst Eng. Comm.* **21** 2431

[23] Boichot R, Coudurier N, Mercier F, Lay S, Crisci A, Coindeau S, Claudel A, Blanquet E and Pons M 2013 *Surf. Coat. Tech.* **237** 118

[24] Kumagai Y, Enatsu Y, Ishizuki M, Kubota Y, Tajima J, Nagashima T, Murakami H, Takada K and Koukitu A 2010 *J. Cryst. Growth* **312** 2530

[25] Hagedorn S, Knauer A, Brunner F, Mogilatenko A, Zeimer U and Weyers M 2017 *J. Cryst. Growth* **479** 16